Analytical Biochemistry 686 (2024) 115406

Contents lists available at ScienceDirect

Analytical Biochemistry

journal homepage: www.elsevier.com/locate/yabio

Comparing *in vitro* affinity measurements of antibodies to TfR1: Surface plasmon resonance versus on-cell affinity

Gillian Bonvicini [a,b], Sunitha Bagawath Singh [a], Patrik Nygren [a], Mengfei Xiong [b], Stina Syvänen [b], Dag Sehlin [b], Ronny Falk [a], Ken G. Andersson [a,*]

[a] BioArctic AB, Warfvinges väg 35, SE-112 51, Stockholm, Sweden
[b] Department of Public Health and Caring Sciences/Geriatrics, Uppsala University, Rudbeck Laboratory, Dag Hammarskjölds väg 20, SE-751 85, Uppsala, Sweden

ARTICLE INFO

Keywords:
Transferrin receptor 1
Surface plasmon resonance
On-cell affinity
Method development
Receptor mediated transcytosis

ABSTRACT

Despite years of utilizing the transferrin receptor 1 (TfR1) to transport large biomolecules into the brain, there is no consensus on how to optimally measure affinity to it. The aim of this study was to compare different methods for measuring the affinities of anti-TfR1 antibodies.

Antibodies 15G11, OX26 and 8D3 are known to successfully carry large biologics across the blood-brain barrier in humans, rats, and mice, respectively. The affinity to their respective species of TfR1 was measured with different surface plasmon resonance setups in Biacore and an on-cell assay.

When the antibody was captured and TfR1 was the analyte, the dissociation in Biacore was very slow. The dissociation was faster when the antibody was the analyte and TfR1 was the ligand. The Biacore setup with capture of N-terminal FLAG-tag TfR1 yielded the most similar apparent affinities as the cell assay.

In conclusion, it is important to evaluate assay parameters including assay orientation, surface capture method, and antibody-format when comparing binding kinetics for TfR1 antibodies. Although it seems possible to determine relative affinities of TfR1 antibodies using the methods described here, both the FLAG-tag TfR1 capture setup and cell assays likely yield apparent affinities that are most translatable *in vivo*.

1. Introduction

A challenge in treating neurodegenerative diseases is that drugs must pass the blood-brain barrier (BBB) to enter the central nervous system. The BBB is the tightly connected cell-layer that separates the brain from the systemic blood circulation. Large molecule drugs, such as antibodies and recombinant proteins, are considered to have attractive half-lives with several days in circulation. However, they are often restricted to peripheral targets as larger biomolecules are most often administered intravenously to patients and do not passively diffuse across the BBB well [1–4]. Some endogenous large molecules can cross the BBB via receptor-mediated transcytosis [5]. Receptor-mediated transcytosis has been utilized for brain delivery of large drug molecules; a strategy known as the molecular Trojan horse [6–11]. Using this strategy, the drug molecule is modified with a protein domain that can bind to an endogenous receptor at the BBB. The modified drug molecule in the blood binds to the receptor on the luminal side of BBB endothelial cells and the whole drug-receptor complex is actively endocytosed. The endosome subsequently travels across the endothelial cell and fuses with the abluminal membrane where the drug molecule is released into the brain.

Transferrin receptor 1 (TfR1) is an especially popular target for this molecular Trojan horse strategy. TfR1 forms a homodimer consisting of two subunits which bind to holo-transferrin (holo-Tf) and thus plays an important role in iron transport into cells and across the BBB (Fig. 1) [12]. Several research groups have successfully targeted TfR1 to carry therapeutic antibodies and recombinant proteins into the brain [6, 13–19]. JCR Pharmaceuticals, Denali Therapeutics and Roche currently have strategies that utilize TfR1-targeting to increase BBB passage of biomolecule drug therapies in clinical trials [20]. In fact, JCR Pharmaceuticals' enzyme replacement therapy for Hunter syndrome utilizing the TfR1-based Trojan horse strategy was approved in Japan in 2021 [21]. Receptor-mediated transcytosis via TfR1 has also been successfully used to improve utility, sensitivity, and accuracy of *in vivo* antibody-based positron emission tomography (PET) radioligands of amyloid-β pathology in rodent models for Alzheimer's disease [2,4,

* Corresponding author.
E-mail address: ken.honek@bioarctic.se (K.G. Andersson).

https://doi.org/10.1016/j.ab.2023.115406
Received 25 July 2023; Received in revised form 13 November 2023; Accepted 18 November 2023
Available online 23 November 2023

22–26].

Affinity to TfR1 influences the efficiency of large molecule drug transport [2,6,16,27]. However, despite many years of investigating TfR1 for the transport of large biomolecules across the BBB, there is no consensus in the field of the optimal way to measure affinity. Affinities have been measured with different techniques (including Biacore, Octet, inhibition ELISA, and radio-receptor assay with mouse fibroblasts), different antigen-formats, and different experimental parameters (such as analyte or ligand concentrations, ligand orientation, and immobilization chemistry) [2,14,16,28–33]. Furthermore, it is difficult to assess the quality of affinity modelling since thorough methods or full sensorgrams are rarely included in the literature. Thus, it is challenging to compare the affinities presented in literature.

The aim of this study was to compare different setups for kinetic analysis of antibodies binding to TfR1. Three antibodies which are known to successfully carry biomolecules across the BBB were investigated: Genentech's anti-human TfR1 antibody, 15G11; publicly available anti-rat TfR1 antibody, OX26; and publicly available anti-mouse TfR1 antibody, 8D3. They are reported to have nanomolar affinities. Characterized in Genentech's patent (#US9708406), the affinity of 15G11 binding to human TfR1 was determined to be 3.3 nM [31]. Affinities range from 2 to 5 nM for OX26 and 0.2–5 nM for 8D3, as has been determined in multiple studies [2,14,16,24,28–30,32].

Here, apparent affinities for these antibodies, in bivalent antibody and monovalent Fab fragment formats, were measured for their respective species of TfR1 (human, rat and mouse) in four different surface plasmon resonance (SPR) setups using Biacore and an on-cell affinity assay. We show that assay parameters, such as assay orientation, surface capture method, and antibody format, have a substantial impact on results and that careful optimization of assays are required. These assay parameters are also important to consider when comparing binding kinetics of TfR1 antibodies.

2. Materials and methods

2.1. Protein production

2.1.1. Recombinant protein expression and purification

The variable regions of the anti-human TfR1 antibody, 15G11, the anti-mouse TfR1 antibody, 8D3, and Genentech's anti-BACE1 antibody as a negative control, were recombinantly expressed with a murine IgG1 backbone. The Fab fragments of 15G11 and 8D3 were recombinantly expressed as a murine kappa light chain with a murine IgG1 CH1 and a 10xHis tag at the C-terminus of the heavy chain. The ectodomains of human TfR1 (C89 to F760), mouse TfR1 (C89 to F763) and rat TfR1 (L101 to F761) were also produced. Human and mouse TfR1 had a 10xHis tag and a TEV cleavage site at the C-terminus while rat TfR1 had a 10xHis tag and a FLAG-tag as described by Thom and colleagues [16]. Human TfR1 (L122 to F760) was also expressed with a 10xHis tag, FLAG-tag, and TEV cleavage site at the N-terminus. GeneArt Elements (ThermoFisher Scientific, Stockholm, Sweden) synthesized pcDNA3.4 expression vectors which were transfected into the Expi293 Expression System (Life Technologies. Carlsbad, USA) as described by Bonvicini et al. [24]. Briefly, Expi293F cells were transfected with 100 μg total of plasmid DNA (1:1 ratio of heavy to light chain for antibodies and Fab fragments) in Opti-MEM® I medium and ExpiFectamine 293 reagent in Opti-MEM® I medium were incubated separately for 5 min. They were mixed, incubated another 10 min, and added to 200 × 10^6 Expi293F cells cultured in Expi293 Expression Medium at 37 °C, 120 RPM, with 70 % humidity and 8 % CO_2. ExpiFectamine 293 Transfection enhancer 1 and 2 were added 20 h later. Cells were harvested 2–3 days later for Fab fragments and TfR1 and 4–5 days for antibodies. On harvest day, cultures were centrifuged at 5000 g for 10 min and the supernatants were filtered through a 0.22 μm filter before purification.

Recombinant proteins were purified with an ÄKTA Purifier system (Cytiva, Uppsala, Sweden). 15G11 and 8D3 were purified on a HiTrap Protein G HP column (Cytiva) and eluted with an increasing gradient of 0.7 % acetic acid. 15G11 Fab, 8D3 Fab and all TfR1 ectodomains were

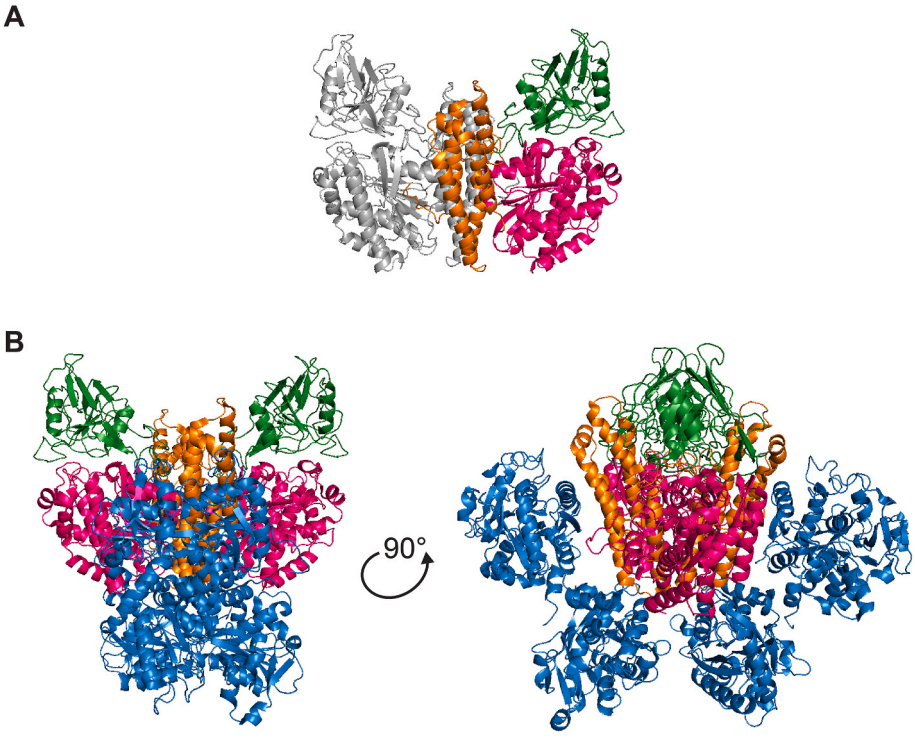

Fig. 1. Schematic of TfR1. (A) Ectodomain of TfR1 homodimer (PDB ID: 1SUV [12]). One subunit is in grey and the other is coloured by domain: the helical domain in orange, the protease-like domain in pink and the apical domain in green. (B) A TfR1 can bind to two transferrins (in blue).

purified on a HisTrap Excel column (Cytiva) with a binding buffer containing 20 mM Tris and 500 mM NaCl and eluted in the binding buffer supplemented with 500 mM imidazole. Following elution, buffer was exchanged to phosphate buffered saline (PBS; Gibco, ThermoFisher Scientific) on a HiPrep 26/10 desalting column. The purity of all recombinant proteins was assessed with SDS-PAGE and all antibodies and Fabs were further assessed with analytical SEC.

2.1.2. Fab fragmentation of OX26

The mouse anti-rat TfR1 antibody, OX26 (LSBio, LS C43741), was purchased and OX26 Fab fragments were prepared using the Pierce™ Fab Preparation Kit (ThermoFisher Scientific). The kit uses immobilized Papain, a nonspecific thiol-endopeptidase, to digest IgG into Fab fragments. Briefly, OX26 (350–400 μg) and immobilized papain resin (125 μl) were incubated in Fab Digestion Buffer supplemented with 3.5 mg/ml cysteine-HCl (pH 7) at 37 °C for 3 h with end-over-end mixing. The digested antibody was separated from the immobilized papain. Fab fragments were purified from Fc fragments and uncleaved antibodies with a Nab Protein A Plus Spin Column and buffer exchanged to PBS with a Zeba spin desalting column (7 K MWCO, ThermoFisher Scientific). Fab purity was assessed with SDS-PAGE.

2.2. Biacore analysis of antibody affinity to TfR1

All SPR experiments were performed on a Biacore 8 K (Cytiva) using HBS-EP+ running buffer (0.01 M HEPES, 0.15 M NaCl, 3 mM EDTA and 0.05 % v/v Surfactant P20, Cytiva). SPR data was analysed with Biacore Insight Evaluation (Cytiva, version 3.0.12.15655). Data was blank subtracted and fit with a 1:1 binding model independent of analyte to visualize potential differences in avidity-induced apparent affinity of the bivalent antibodies and to be comparable to the apparent affinity determined in the cell assay.

2.2.1. Antibody capture with injection of TfR1 as analyte

A 5-step single cycle kinetics (SCK) analysis with capture on an anti-mouse antibody chip was performed as previously described (Fig. 2A) [24]. Briefly, a mouse antibody capture chip was generated using the Mouse Antibody Capture Kit, type 2 (Cytiva) on a CM5 chip (Cytiva) according to the manufacturer's instructions. Antibodies (15G11, OX26, 8D3 or the negative control, 10 μg/ml) were captured on flow cell 2. Flow cell 1 was regenerated with 3 M $MgCl_2$ for 60 s and a 60 s wait step to ensure that no antibody was captured on the reference flow cell. Serial dilutions of TfR1 (human and mouse: 2-fold, 3.1–50 nM; rat: 4-fold, 3.2–2000 nM) were injected over both flow cells. Association was measured for 120 s/concentration and the dissociation for 1800 s before regeneration with 3 M $MgCl_2$.

2.2.2. Immobilized TfR1 as ligand with injections of antibody or Fab as analyte

To flip the orientation, human, rat, or mouse TfR1 was immobilized on a CM5 sensor chip according to manufacturer's instructions using the Amine Coupling Kit (Cytiva) (Fig. 2B). Both flow cells were activated with 1:1 v/v solution of 1-ethyl-3-(3-dimethylaminopropyl)carbodiimide hydrochloride (EDC) and N-hydroxysuccinimide (NHS). TfR1 (human: 1.5 μg/ml; rat: 3 μg/ml or mouse: 3 μg/ml) in 10 mM sodium acetate (pH 5.5) was immobilized on flow cell 2. Both flow cells were capped with ethanolamine-HCl. Different concentrations of TfR1 were used to ensure similar immobilization levels of 1579 ± 149 RU for all ligands. Maintained human TfR1 activity was controlled with a single injection of human holo-Tf (100 nM; Sigma-Aldrich, St. Louis, USA).

Antibodies 15G11, OX26, 8D3 in IgG or Fab formats and the negative control antibody were injected over both flow cells in a 5-step SCK analysis in a serial 2-fold dilution from 3.1 to 50 nM. Each association step was 160 s and the dissociation was 300 s. Surfaces were regenerated with 4 M NaCl followed by a 3600 s wait step.

2.2.3. FLAG-tag TfR1 capture with IgG or Fab injected as analyte

To ensure a uniform surface, a 5-step SCK analysis with capture of N-terminal FLAG-tag human TfR1 was performed (Fig. 2C). A FLAG-tag capture chip was generated by immobilizing anti-FLAG-tag antibody (FG4R, ThermoFisher; 10 μg/ml in 10 mM sodium acetate, pH 4.5) on both flow cells of a CM3 sensor chip (Cytiva) with the Amine Coupling Kit. N-terminal FLAG-tag human TfR1 (5 μg/ml) was captured on flow cell 2. Serial 2-fold dilutions of 15G11 (1.6–25 nM), 15G11 Fab (3.1–50 nM), and the negative control antibody (1.6–25 nM) were injected over both flow cells at 15 μl/min. Each association step was 120 s and the dissociation step was 300 s. Surfaces were regenerated with 10 mM glycine-HCl, pH 2.5.

2.2.4. Immobilized holo-hTf with TfR1 capture and IgG or Fab analyte

To measure apparent affinity against the holo-Tf/TfR1 complex, a 5-step SCK analysis with capture of human TfR1 to immobilized holo-Tf was performed (Fig. 2D). Holo-Tf (10 μg/ml in 10 mM sodium acetate, pH 5.5) was immobilized on both flow cells of a CM5 sensor chip with the Amine Coupling Kit. Human TfR1 (0.5 μg/ml) was captured on flow cell 2. Serial 2-fold dilutions of 15G11 (1.6–25 nM), 15G11 Fab (3.1–50 nM), and the negative control antibody (1.6–25 nM) were injected over both flow cells at 15 μl/min. Association was measured for 120 s/concentration and dissociation for 300 s. Surfaces were regenerated with 3 M $MgCl_2$.

2.3. Cell assay for determining TfR1 apparent affinity

Apparent affinities of 15G11 and 8D3 (antibody and Fab) to TfR1 were also measured on immortalized cerebral endothelial cell lines: hCMEC/D3 cells (Sigma-Aldrich) for 15G11 binding to human TfR1 and cEND cells (Applied Biological Materials Inc., Richmond, Canada) for 8D3 binding to mouse TfR1 (Fig. 2E). Cells were cultured in a humidified incubator at 37 °C with 10 % CO_2. hCMEC/D3 cells were cultured in Endothelial Cell Growth Medium 2 (PromoCell GmbH, Heidelberg, Germany) and cEND cells in Gibco DMEM medium (ThermoFisher Scientific). For the affinity assay, cells were trypsinized wih TripLE express

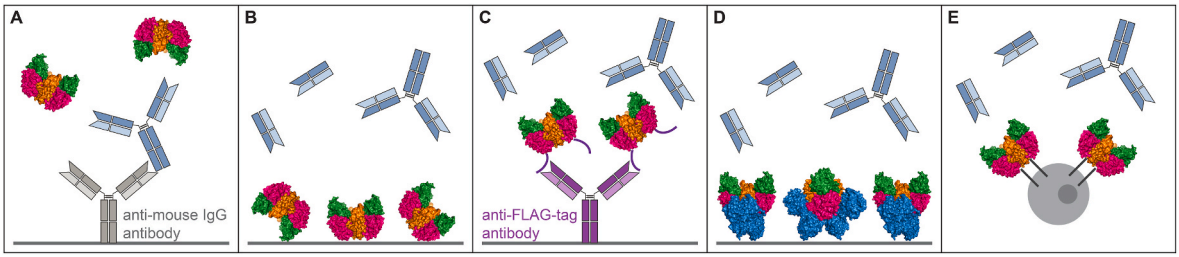

Fig. 2. Schematic of different kinetic assay setups in Biacore and on cell. Biacore kinetic assays where (A) the anti-TfR1 antibody is captured using an anti-mouse IgG and TfR1 was used as analyte, (B) TfR1 is immobilized on the chip to measure the kinetic parameters of either antibody or Fab, (C) TfR1 with an N-terminal FLAG-tag is captured on the surface with an anti-FLAG-tag antibody to ensure uniform TfR1 orientation, and (D) functional TfR1 is captured with immobilized holo-Tf. (E) An on-cell assay determines the apparent affinity to TfR1 in an *in vivo*-like conformation.

enzyme (ThermoFisher Scientific) and centrifuged for 5 min at 1200 RPM. The pellet was resuspended in PBS and 0.3 million viable cells were added to each well of a 96 well U bottom plate. The PBS was discarded and cells were blocked for 20 min with Fc receptor blocker (NB309, Innovex Biosciences Inc., Richmond, USA). 15G11 IgG and Fab were serially diluted from 200 nM to 10.1 pM and 8D3 IgG or Fab from 500 nM to 8.5 pM. Cells incubated with the test antibodies for 30 min at 4 °C before being washed twice with PBS. AlexaFlour 647 AffiniPure goat-*anti*-mouse IgG F(ab')$_2$ fragment secondary antibody (1:300 in PBS, #115-605-006, Jackson ImmunoResearch, Pennsylvania, USA) was applied to the cells and incubated for 30 min at 4 °C. After incubation, cells were washed twice and resuspended in 200ul of PBS. The fluorescent signal was measured with BD FACSLyric Flow Cytometry System (BD Biosciences, San Jose, CA) and data were analysed with FlowJo, version 10.8.1 (BD Biosciences). Mean fluorescent intensity (MFI) was subtracted from MFI of only secondary as background control samples. Background corrected MFI was plotted against the antibody concentration for two replicates. With GraphPad Prism 9.5.0 (GraphPad Software, Inc.), concentrations were transformed to logarithms and EC50 values were calculated with the log(agonist) vs response – variable slope (four parameters) curve fit. EC50 values were used as a surrogate for apparent affinity since the maximal response measured in this assay was saturation of binding sites on the cell surface.

3. Results

3.1. Antibody binding and selectivity to three species of TfR1

The conventional setup in Biacore to measure an antibody's affinity to its antigen is to have the antibody as the ligand and the antigen as the analyte. Using an antibody capture setup, 15G11, OX26, and 8D3 affinity and species selectivity to human, rat, and mouse TfR1 were determined. 15G11 bound to human TfR1 with high affinity driven by a fast association but did not bind to either rat or mouse TfR1 (Fig. 3, Table 1). Both OX26 and 8D3 bound to rat and mouse TfR1 respectively with high affinity and had the same level of selectivity when presented with the three TfR1 species. Unlike 15G11, the high affinities of OX26 and 8D3 were driven by a slow dissociation. No binding of TfR1 was detected when injections were made over the negative control (Supplemental Fig. 1A).

3.2. Faster dissociations with TfR1 as the ligand

The conventional antibody affinity setup was then compared to a setup where the ligand and the analyte were switched (i.e. the TfR1 was immobilized on the chip and either the antibodies or Fab fragments were injected over the surface). Using this assay setup, binding was detected with all antibodies and Fabs to their respective TfR1 (Fig. 4A), while no binding could be detected with the negative control on any of the surfaces (Supplemental Fig. 1B). The apparent affinity for 8D3 was 31-fold lower when mouse TfR1 was immobilized on the surface than when mouse TfR1 was used as the analyte, due to the dissociation rate being 2 orders of magnitude slower. The apparent affinities for 15G11 and OX26 were very similar between the two setups, although the apparent affinities for both antibodies were slightly higher when TfR1 was immobilized (Table 1). When injected over the immobilized TfR1, the affinities for the Fabs were consistently lower than the apparent affinities for the three antibodies (8.1-fold for 15G11, 11-fold for OX26, and 19-fold for 8D3). There was also a marked difference in the dissociation rate constants between the Fab and the antibody, for all three antibodies (7.5-fold for 15G11, 4.8-fold for OX26, and 24-fold for 8D3, Table 1).

To measure antibody binding to a TfR1-surface with a more directed orientation of the ligand, a Biacore setup employing anti-FLAG capture of N-terminal FLAG-tag TfR1 was used (Fig. 4B). The orientation of human TfR1 did not impact the affinity of 15G11 Fab but it did have a large effect on the apparent affinity of the antibody (Table 1). The apparent affinity of 15G11 in the FLAG-tag TfR1 setup was 3.4-fold lower than when human TfR1 was immobilized. There was still a

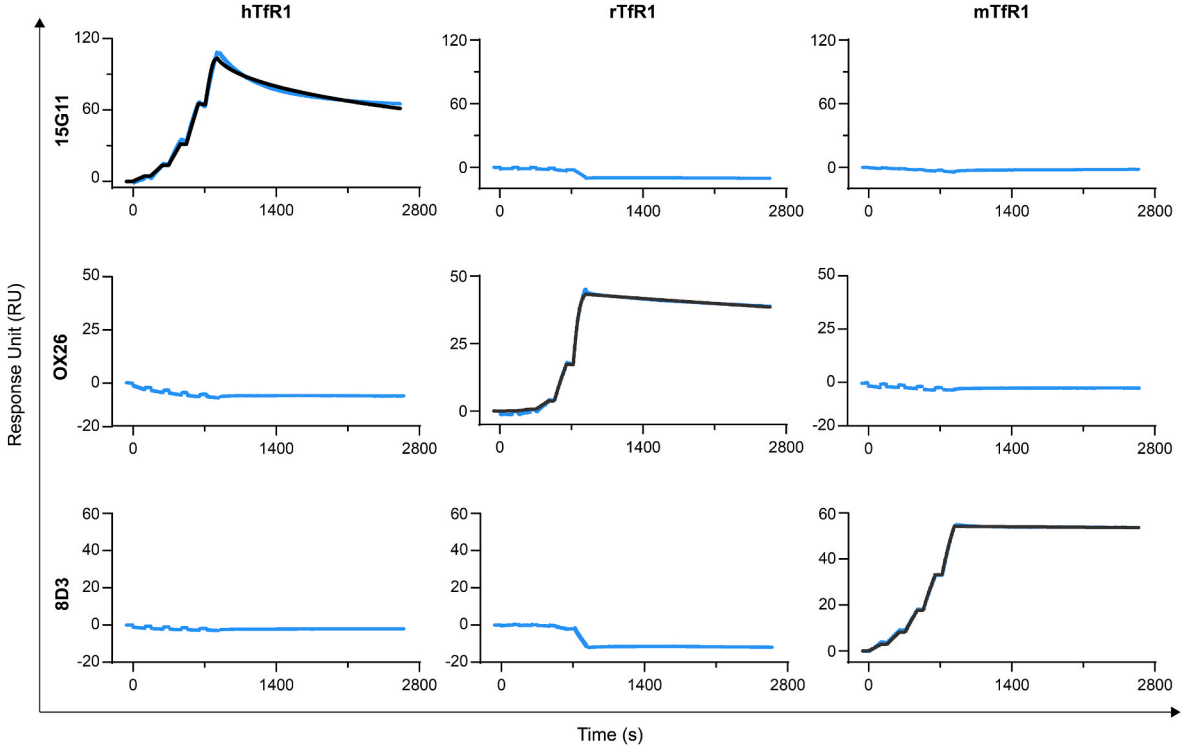

Fig. 3. Affinity determination using Biacore with TfR1 as analyte. Analysis of TfR1 (human, rat, and mouse, left to right) binding to 15G11, OX26, and 8D3 (top to bottom). Antibodies were captured on the chip and TfR1 was used as the analyte for SCK analysis. Representative, blank subtracted sensorgrams in blue and 1:1 fitted curves in black.

Table 1
Antibody binding kinetics to TfR1 in different Biacore kinetic assays and an on-cell affinity assay.

TfR1	Antibody	IgG			Fab		
		k_a ($M^{-1}s^{-1}$)	k_d (s^{-1})	K_D (nM)	k_a ($M^{-1}s^{-1}$)	k_d (s^{-1})	K_D (nM)
Antibody captured							
human	15G11	1.17×10^6	8.84×10^{-4}	0.75	–	–	–
rat	OX26	1.69×10^4	6.05×10^{-5}	3.61	–	–	–
mouse	8D3	7.22×10^4	3.87×10^{-6}	0.05	–	–	–
Immobilized TfR1							
human	15G11	$2.57 \pm 0.05 \times 10^5$	$2.12 \pm 0.38 \times 10^{-4}$	0.82 ± 0.15	$2.39 \pm 0.13 \times 10^5$	$1.58 \pm 0.03 \times 10^{-3}$	6.66 ± 0.46
rat	OX26	$5.72 \pm 0.07 \times 10^4$	$1.27 \pm 0.01 \times 10^{-4}$	2.23 ± 0.04	$2.62 \pm 0.33 \times 10^4$	$6.12 \pm 0.11 \times 10^{-4}$	23.6 ± 3.02
mouse	8D3	2.08×10^5	3.24×10^{-4}	1.56	2.55×10^5	7.70×10^{-3}	30.3
N-terminal FLAG-tag capture of TfR1							
human	15G11	$5.74 \pm 0.68 \times 10^5$	$1.61 \pm 0.38 \times 10^{-3}$	2.80 ± 0.58	$4.18 \pm 0.34 \times 10^5$	$2.98 \pm 0.45 \times 10^{-3}$	7.12 ± 0.73
TfR1 captured with immobilized holo-Tf							
human	15G11	$6.94 \pm 0.30 \times 10^5$	$7.85 \pm 0.82 \times 10^{-4}$	1.13 ± 0.08	$6.56 \pm 1.13 \times 10^5$	$2.06 \pm 0.34 \times 10^{-3}$	3.21 ± 0.77

On-cell TfR1 apparent affinity assay	Human TfR1 on D3 cells		Mouse TfR1 on cEND cells	
	IgG	Fab	IgG	Fab
EC50 (nM)	3.19 (2.85–3.60)	5.89 (5.36–6.55)	3.05 (2.25–4.27)	28.7 (22.9–37.8)

Values represent mean of 2 replicates for the antibody capture setup or mean ± SD of 3–9 replicates for the other Biacore setups. The on-cell data is the EC50 (95 % CI) for a curve fit to 2 replicates.

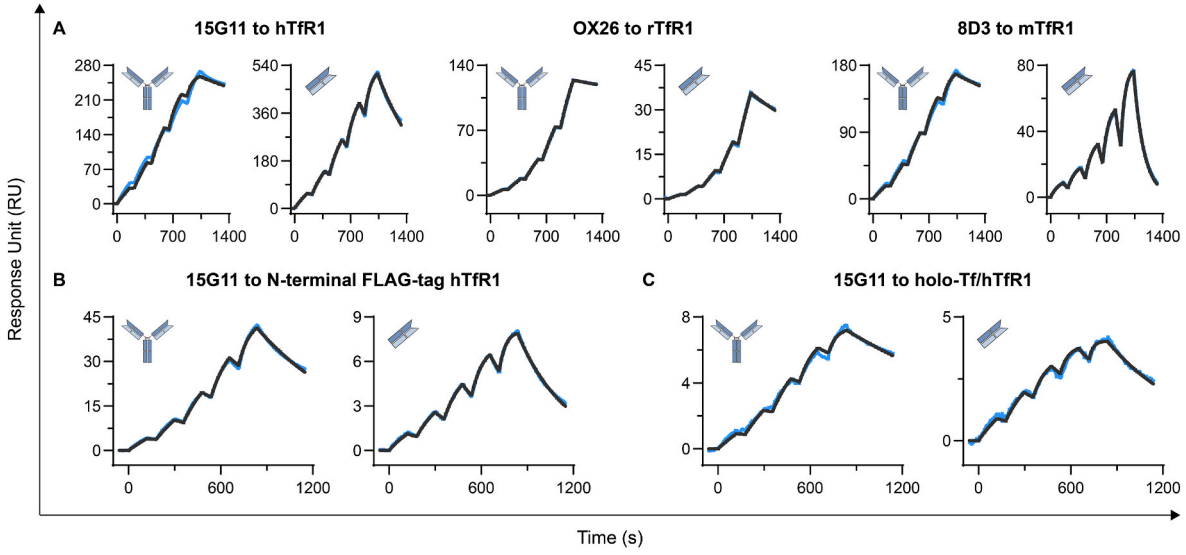

Fig. 4. Affinity determination using Biacore with TfR1 as the ligand. Affinity analysis with (A) immobilized TfR1, (B) N-terminal FLAG-tag TfR1 captured on a FLAG-tag capture chip, and (C) TfR1 captured with immobilized holo-Tf. Representative, blank subtracted sensorgrams in blue and 1:1 fitted curves in black.

difference in the apparent affinities of the antibody and the 15G11 Fab when binding to the FLAG-tag captured human TfR1, with the affinity of the 15G11 Fab being 2.5-fold lower than the 15G11 apparent affinity. This difference was due to small differences in both the association and dissociation.

A final Biacore setup to measure 15G11 antibody and Fab binding to the holo-Tf/TfR1 complex was performed by capturing human TfR1 with human holo-Tf immobilized on the sensor chip (Fig. 4C). The relative differences in the apparent affinities of 15G11 and the 15G11 Fab was similar with this setup (2.8-fold lower for the 15G11 Fab) as with the FLAG-tag captured human TfR1 setup. However, the apparent affinity for both 15G11 and the 15G11 Fab were ~2-fold higher to the holo-Tf/TfR1 complex than to the human TfR1 captured via the FLAG-tag (2.5-fold for 15G11 and 2.2-fold for 15G11 Fab; Table 1). No binding of the negative control was detected to the FLAG-tag captured human TfR1 or the human TfR1 captured with the holo-Tf (Supplemental Figs. 1C and D)

3.3. Apparent affinity determined on human and mouse endothelial cell lines corresponded to the affinity differences between Fab and IgG measured in Biacore

The on-cell apparent affinities of 15G11 and 15G11 Fab to human TfR1 were measured using hCMEC/D3 cells and for 8D3 and 8D3 Fab to mouse TfR1 using cEND cells (Fig. 5, Table 1). The antibodies had higher on-cell apparent affinities to TfR1 than the respective Fab, 1.8-fold higher for 15G11 and 9.4-fold higher for 8D3 (Table 1). The on-cell apparent affinity was lower than the apparent affinity determined using the antibody capture setup in Biacore for both 15G11 and 8D3 (2.7-fold for human, 61-fold for mouse). The on-cell apparent affinities for the 15G11 and 8D3 Fabs were similar to the affinities of the Fabs binding to the immobilized TfR1 while the apparent affinities for the antibodies were 2-4-fold lower on cell than to immobilized TfR1. Both the on-cell 15G11 and 15G11 Fab apparent affinities were similar to the apparent affinity for 15G11 and the affinity for 15G11 Fab determined

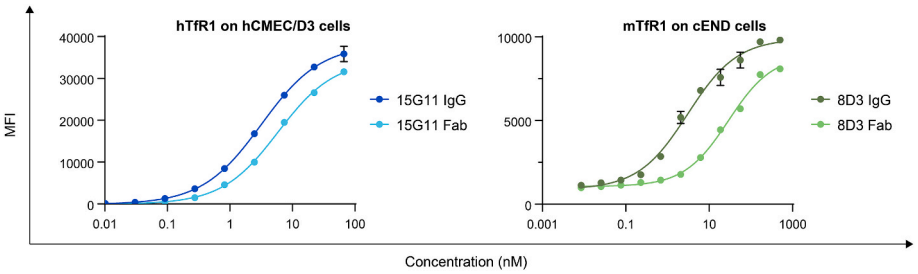

Fig. 5. Determination of apparent affinity to TfR1 on cells. Affinity analysis of 15G11 IgG and Fab binding to human TfR1 on hCMEC/D3 cells (left) and 8D3 IgG and Fab binding to mouse TfR1 on cEND cells (right).

in Biacore with TfR1 captured via the FLAG-tag setup. The on-cell apparent affinities were lower than the values measured in the holo-Tf/TfR1 complex setup: the on-cell apparent affinity of 15G11 was 2.8-fold lower than that measured in Biacore and the 15G11 Fab had a 1.8-fold lower on-cell apparent affinity than the Biacore affinity. The antibody-to-Fab relationship for 15G11 binding to human TfR1 on cells was 4.5-fold higher than the relationship for 15G11 binding to immobilized TfR1 while the relationship was similar in the on-cell assay and both the anti-FLAG tag and the holo-Tf/TfR1 capture setups in Biacore.

4. Discussion

The aim of this study was to compare different experimental setups for measuring antibody affinity to TfR1 with SPR (Biacore) and to compare the values with an on-cell assay. Three anti-TfR1 antibodies which bind the apical TfR1 domain and are known to function as BBB transporters for large molecule drugs in humans, rats or mice were used: 15G11, OX26 and 8D3, respectively [13,14,31]. Extensive investigation of OX26 and 8D3 indicates that they can enhance transport efficiency into the brain of differently formed large molecule cargo (including nanoparticles, enzymes, bispecific antibodies, and antibody-fragments) for therapeutic and PET diagnostic purposes [2–4,16,22–24,29,34–36]. As a gold standard for determining kinetic parameters in real-time [37], Biacore was used to measure the apparent affinity of 15G11, OX26 and 8D3 to their respective species of TfR1 with four different setups: 1) antibody capture; 2) immobilized TfR1; 3) FLAG-tag capture of TfR1; and 4) TfR1 captured with immobilized holo-Tf. Apparent affinities for 15G11 and 8D3 were also measured in an on-cell assay. Cell assays for determining affinity provide a unique setup in which parameters such as receptor density, conformation, and orientation mimic *in vivo* conditions [38].

In Biacore, antibody affinity to its target is typically measured with the antibody as the ligand and the antigen as the analyte. This setup removes common avidity contributions to an interaction that a bivalent antibody can display when it binds to an immobilized target. However, this is only the case if the injected antigen is a monomer with a single epitope for the antibody. Measuring affinity against a multimeric target or a target with repeating epitopes is difficult. It introduces the risk of measuring avidity since an antigen with more than one epitope could bind to the surface multiple times. Avidity will result in a higher apparent affinity than the affinity from a 1:1 interaction. In the capture assay, the apparent affinity of rat TfR1 binding to OX26 measured here fell within the reported affinity range of 2–5 nM [16,24,30]. Measurements with human TfR1 binding to 15G11 indicated that the apparent affinity was slightly higher than the 3.3 nM affinity reported in Genentech's patent [31]. The apparent affinity of mouse TfR1 binding to 8D3, however, was substantially higher than the previously reported affinity range of 0.2–5 nM [2,14,28–30,32]. The majority of studies reporting affinity for unmodified, bivalent 8D3 use other methods such as an inhibition ELISA or a radio-receptor assay binding to TfR on mouse fibroblasts making it difficult to directly compare affinities. Webster and colleagues did measure affinity in Biacore with the antibody as the ligand. They report an affinity of 1.2 nM with a dissociation rate constant of 1.1×10^{-4} s^{-1}, which was 2 orders of magnitude slower than our dissociation rate constant. In contrast, the apparent affinity for both 15G11 and 8D3 determined with our cell assay matched the reported affinities. The discrepancies between our data collected using the antibody capture setup and the previous studies using the mouse TfR1 could be due to the TfR1 forming complexes, such as dimers, during the course of the experiment which would affect the measured apparent affinities due to avidity effects [39]. An antibody used as an analyte will bind bivalently in a 1:2 binding stoichiometry while an analyte prone to multimerization will have an unknown number of interactions likely yielding a binding stoichiometry higher than 2. The higher apparent affinity and slower dissociation seen in the antibody capture setup compared to the literature and the cell assay confirm this hypothesis. Further studies could evaluate if it is possible to reduce, or remove, the avidity effect by titrating the amount of 8D3 used for the capture or by using other TfR1 variants such as the soluble isolated apical domain of TfR1 [33,40,41].

Since there were indications of complexes of TfR1 forming when used as an analyte, we decided to investigate if it would be possible to generate more reliable binding data by using the TfR1 as the ligand. The orientation of the binding interaction substantially affected the apparent affinity of 8D3 to mouse TfR1 while having limited effect on the apparent affinity of 15G11 to human TfR1 and of OX26 to rat TfR1. The dissociation rate was the main differing kinetic parameter between each IgG and Fab, confirming that the valency of the antigen was the major contributor to apparent affinity differences.

The apparent affinity IgG-to-Fab relationship for 15G11 was substantially smaller than for 8D3 in both the Biacore direct immobilized TfR1 setup and on-cell assay, suggesting that some antibodies (*e.g.* 8D3) display more avidity effect than others (*e.g.* 15G11). This was unexpected since these antibodies have many similarities: they were both developed in hybridomas, both bind to the TfR1 apical domain, and both have similar apparent affinities to their respective TfR1 species [29,31,42].

In the setup with immobilized TfR1, the Fab fragments of all three antibodies interacted monovalently with the receptor which is optimal for determining affinity. The affinities determined for the 15G11 and 8D3 Fabs binding to immobilized TfR1 corresponded well with apparent affinities from the on-cell assay. In contrast, both 15G11 and 8D3 bound to TfR1 with a higher apparent affinity in the immobilized TfR1 setup than in the on-cell assay. Therefore, the immobilized TfR1 setup described here is likely better suited for measuring interactions of truly monovalent binders to TfR1, such as the Fab fragments. This setup is still a relevant Biacore setup for the TfR1-mediated drug delivery field since monovalent binders are thought to cross the BBB more efficiently and safely than bivalent binders [2,15,43]. Further optimization may be achieved by titrating down the immobilization levels to reach a surface density like that on cells which may yield more similar apparent affinities for bivalent antibodies. Another limitation with this setup is that TfR1 was immobilized on the surface via NHS-coupling. Since NHS-coupling is a primary amine-directed conjugation, it typically

generates a random, heterogenous surface. Therefore, we explored two different ways to create a more uniform surface.

In the first setup with a more uniform surface, human TfR1 with an N-terminal FLAG-tag was captured on an anti-FLAG-tag chip to obtain uniformly oriented TfR1 comparable to the orientation on the cell surface. The apparent affinities measured for 15G11 and the Fab in this setup were comparable and, notably, had almost identical dissociation rates indicating that there was a limited contribution of avidity binding of 15G11. The apparent affinities from this Biacore setup also corresponded well with the EC50 of the TfR-specific on-cell saturation *i.e.*, on-cell apparent affinities, suggesting that the apparent affinities measured here are better translatable to *in vivo* conditions. An extra benefit of this Biacore setup over the cell assay is that kinetic parameters of the apparent affinity are also measured with Biacore. Other methods would need to be employed to measure kinetic parameters on cells. For example, one could use LigandTracer where the antibody is radiolabelled for detection while interacting with cells coated on a plate. This method provides similar sensorgrams as the Biacore but has the limitation that the radiolabelling process can negatively affect the affinity of the antibody.

In the second setup, human TfR1 was captured with immobilized human holo-Tf. This assay provides two benefits: it can test if the antibody epitope competes with the receptor's endogenous ligand, and it measures apparent affinities to functional TfR1 molecules which can bind to holo-Tf. The kinetic parameters for 15G11 and the Fab were different between the FLAG-tag TfR1 capture and holo-Tf capture setups. The antibody and Fab apparent affinities measured against the holo-Tf/TfR1 complex were also stronger than the apparent affinities measured in the FLAG-tag capture setup and the cell assay. This could indicate that binding of Tf to TfR1 introduces a conformational change or a sterical hindrance to TfR1, which would be unexpected since the apical domain is structurally conserved in TfR1 crystal structures with or without Tf bound [12,44]. The 15G11 antibody-to-Fab apparent affinities relationship was similar in both Biacore setups (2.5-fold difference for the FLAG-tag chip and 2.8-fold difference for the holo-Tf chip). Therefore, although the holo-Tf/TfR1 complex setup may not be ideal for determining exact affinities, it could be useful for providing relative affinities and exploring potential affinity differences upon Tf binding.

SPR, and Biacore in particular, is a commonly used technique for measuring kinetic parameters and for reporting affinities. There are numerous other techniques that can be employed to measure protein-protein interactions, and thereby further shed light on TfR1 binding. Affinity determination could, for example, be performed using Microfluidic Diffusional Sizing (MDS), Microscale Thermophoresis (MST) and Isothermal Titration Calorimetry (ITC) in solution. MST and ITC can measure interactions of native proteins, whereas MDS require labelling of either the antigen or the antibody (MST is greatly aided by labelling) which could affect the interaction depending on where the label is introduced. All three techniques offer high sensitivity, and both MDS and MST can detect binding in complex mixtures such as cell supernatant. In addition to the K_D, these techniques provide useful information about, for example, the thermodynamic parameters, size, and stoichiometry, giving a more comprehensive understanding of the TfR1 binding, although they do not provide real-time kinetic information.

5. Conclusions

In conclusion, we have described several methods for measuring the apparent affinity of antibodies to TfR1. Assay parameters, including assay orientation, surface capture method, and antibody-format, can have a large impact on kinetic parameters measured. It seems possible to reliably determine relative affinities of antibodies using any of the Biacore setups described here with TfR1 as the ligand. Which method is best suited will depend on the specific aim of future scientific questions. Absolute affinity determination is challenging, as was expected from the few thorough reports in literature. Both the N-terminal FLAG-tag TfR1 capture and on-cell assay yielded similar apparent affinities, suggesting that a directional and uniform capture approach setup in Biacore may be ideal for both measuring kinetic parameters and emulating *in vivo* conditions.

Consent for publication

Not applicable.

Availability of data and materials

The datasets used and/or analysed during the current study are available from the corresponding author on reasonable request.

Funding

This work was supported by the European Union's Horizon 2020 research and innovation programme under the Marie Skłodowska-Curie (grant agreement No 813528). The funding organization did not take part in the study design, the collection, analysis, and interpretation of data, in writing the manuscript, or the decision to submit the article for publication.

Gillian Bonvicini: conceptualization, methodology, validation, formal analysis, investigation, writing – original draft, visualization. **Sunitha Singh:** investigation, writing – reviewing and editing. **Patrik Nygren:** supervision, writing – reviewing and editing. **Mengfei Xiong:** methodology, writing – reviewing and editing. **Stina Syvänen:** supervision, writing – reviewing and editing. **Dag Sehlin:** supervision, writing – reviewing and editing. **Ronny Falk:** conceptualization, resources, supervision, writing – reviewing and editing. **Ken G. Andersson:** conceptualization, resources, supervision, writing – reviewing and editing.

Declaration of competing interest

The authors declare the following financial interests/personal relationships which may be considered as potential competing interests: Gillian Bonvicini, Sunitha Singh, Patrik Nygren, Ronny Falk, and Ken G. Andersson are employees of BioArctic AB, Sweden.

The other authors declare that they have no competing interests.

Data availability

Data will be made available on request.

Acknowledgements

We thank Lisa Sandersjöö and Josefine Karlsson for protein production support. Graphical abstract was made in part with BioRender.

Appendix A. Supplementary data

Supplementary data to this article can be found online at https://doi.org/10.1016/j.ab.2023.115406.

Abbreviations

BBB	blood-brain barrier
EDC	3-(3-dimethylaminopropyl)carbodiimide hydrochloride
holo-Tf	holo-transferrin
ITC	Isothermal Titration Calorimetry
k_a	association rate constant
k_d	dissociations rate constant
K_D	equilibrium dissociation constant
MFI	mean fluorescent intensity
MDS	Microfluidic Diffusional Sizing

MST	Microscale Thermophoresis
NHS	N-hydroxysuccinimide
PBS	phosphate buffered saline
PET	positron emission tomography
SCK	single cycle kinetics
SD	standard deviation
SPR	surface plasmon resonance
TfR1	transferrin receptor 1

References

[1] K. Magnusson, D. Sehlin, S. Syvänen, M.M. Svedberg, O. Philipson, L. Söderberg, K. Tegerstedt, M. Holmquist, P. Gellerfors, V. Tolmachev, G. Antoni, L. Lannfelt, H. Håkanall, L.N.G. Nilsson, Specific uptake of an amyloid-β protofibril-binding antibody-tracer in AβPP transgenic mouse brain, J. Alzheim. Dis. 37 (2013) 29–40, https://doi.org/10.3233/JAD-130029.

[2] G. Hultqvist, S. Syvänen, X.T. Fang, L. Lannfelt, D. Sehlin, Bivalent brain shuttle increases antibody uptake by monovalent binding to the transferrin receptor, Theranostics 7 (2017) 308–318, https://doi.org/10.7150/thno.17155.

[3] S. Syvänen, G. Hultqvist, T. Gustavsson, A. Gumucio, H. Laudon, L. Söderberg, M. Ingelsson, L. Lannfelt, D. Sehlin, Efficient clearance of Aβ protofibrils in AβPP-transgenic mice treated with a brain-penetrating bifunctional antibody, Alzheimer's Res. Ther. 10 (2018) 1–10, https://doi.org/10.1186/s13195-018-0377-8.

[4] D. Sehlin, P. Stocki, T. Gustavsson, G. Hultqvist, F.S. Walsh, J.L. Rutkowski, S. Syvänen, Brain delivery of biologics using a cross-species reactive transferrin receptor 1 VNAR shuttle, FASEB (Fed. Am. Soc. Exp. Biol.) J. 34 (2020) 13272–13283, https://doi.org/10.1096/fj.202000610RR.

[5] K.B. Johnsen, A. Burkhart, L.B. Thomsen, T.L. Andresen, T. Moos, Targeting the transferrin receptor for brain drug delivery, Prog. Neurobiol. 181 (2019) 1–30, https://doi.org/10.1016/j.pneurobio.2019.101665.

[6] Y.J. Yu, Y. Zhang, M. Kenrick, K. Hoyte, W. Luk, Y. Lu, J. Atwal, J.M. Elliott, S. Prabhu, R.J. Watts, M.S. Dennis, Boosting brain uptake of a therapeutic antibody by reducing its affinity for a transcytosis target, Sci. Transl. Med. 3 (2011) 1–9, https://doi.org/10.1126/scitranslmed.3002230.

[7] Z. Zhao, B.V. Zlokovic, Therapeutic TVs for crossing barriers in the brain, Cell 182 (2020) 267–269, https://doi.org/10.1016/j.cell.2020.06.041.

[8] R.J. Boado, E.K.W. Hui, J.Z. Lu, R.K. Sumbria, W.M. Pardridge, Blood-brain barrier molecular trojan horse enables imaging of brain uptake of radioiodinated recombinant protein in the rhesus monkey, Bioconjugate Chem. 24 (2013) 1741–1749, https://doi.org/10.1021/bc400319d.

[9] R.J. Boado, Y. Zhang, Y. Zhang, C.F. Xia, Y. Wang, W.M. Pardridge, Genetic engineering of a lysosomal enzyme fusion protein for targeted delivery across the human blood-brain barrier, Biotechnol. Bioeng. 99 (2008) 475–484, https://doi.org/10.1002/bit.21602.

[10] R.J. Boado, W.M. Pardridge, Brain and organ uptake in the Rhesus monkey in vivo of recombinant iduronidase compared to an insulin receptor antibody-iduronidase fusion protein, Mol. Pharm. 14 (2017) 1271–1277, https://doi.org/10.1021/acs.molpharmaceut.6b01166.

[11] T. Morito, R. Harada, R. Iwata, Y. Du, N. Okamura, Y. Kudo, K. Yanai, Synthesis and pharmacokinetic characterisation of a fluorine-18 labelled brain shuttle peptide fusion dimeric affibody, Sci. Rep. 11 (2021) 1–12, https://doi.org/10.1038/s41598-021-82037-2.

[12] Y. Cheng, O. Zak, P. Aisen, S.C. Harrison, T. Walz, N. York, Structure of the human transferrin receptor-transferrin complex albert einstein college of medicine, Cell 116 (2004) 565–576. http://www.ncbi.nlm.nih.gov/pubmed/14980223.

[13] P.M. Friden, L.R. Walus, G.F. Musso, M.A. Taylor, B. Malfroy, R.M. Starzyk, Anti-transferrin receptor antibody and antibody-drug conjugates cross the blood-brain barrier, Proc. Natl. Acad. Sci. U.S.A. 88 (1991) 4771–4775, https://doi.org/10.1073/pnas.88.11.4771.

[14] R.J. Boado, Y. Zhang, Y. Wang, W.M. Pardridge, Engineering and expression of a chimeric transferrin receptor monoclonal antibody for blood-brain barrier delivery in the mouse, Biotechnol. Bioeng. 102 (2009) 1251–1258, https://doi.org/10.1002/bit.22135.

[15] J. Niewoehner, B. Bohrmann, L. Collin, E. Urich, H. Sade, P. Maier, P. Rueger, J. O. Stracke, W. Lau, A.C. Tissot, H. Loetscher, A. Ghosh, P.O. Freskgård, Increased brain penetration and potency of a therapeutic antibody using a monovalent molecular shuttle, Neuron 81 (2014) 49–60, https://doi.org/10.1016/j.neuron.2013.10.061.

[16] G. Thom, M. Burrell, A.S. Haqqani, A. Yogi, E. Lessard, E. Brunette, C. Delaney, E. Baumann, D. Callaghan, N. Rodrigo, C.I. Webster, D.B. Stanimirovic, Enhanced delivery of galanin conjugates to the brain through bioengineering of the anti-transferrin receptor antibody OX26, Mol. Pharm. 15 (2018) 1420–1431, https://doi.org/10.1021/acs.molpharmaceut.7b00937.

[17] C.R. Campos, A.M. Kemble, J. Niewoehner, P.O. Freskgård, E. Urich, Brain shuttle neprilysin reduces central amyloid-β levels, PLoS One 15 (2020) 1–12, https://doi.org/10.1371/journal.pone.0229850.

[18] J.C. Ullman, A. Arguello, J.A. Getz, A. Bhalla, C.S. Mahon, J. Wang, T. Giese, C. Bedard, D.J. Kim, J.R. Blumenfeld, N. Liang, R. Ravi, A.A. Nugent, S.S. Davis, C. Ha, J. Duque, H.L. Tran, R.C. Wells, S. Lianoglou, V.M. Daryani, W. Kwan, H. Solanoy, H. Nguyen, T. Earr, J.C. Dugas, M.D. Tuck, J.L. Harvey, M.L. Reyzer, R. M. Caprioli, S. Hall, S. Poda, P.E. Sanchez, M.S. Dennis, K. Gunasekaran, A. Srivastava, T. Sandmann, K.R. Henne, R.G. Thorne, G. Di Paolo, G. Astarita, D. Diaz, A.P. Silverman, R.J. Watts, Z.K. Sweeney, M.S. Kariolis, A.G. Henry, Brain delivery and activity of a lysosomal enzyme using a blood-brain barrier transport vehicle in mice, Sci. Transl. Med. 12 (2020) 1–13, https://doi.org/10.1126/scitranslmed.aay1163.

[19] R. Giugliani, A.M. Martins, S. So, T. Yamamoto, M. Yamaoka, T. Ikeda, K. Tanizawa, H. Sonoda, M. Schmidt, Y. Sato, Iduronate-2-sulfatase fused with anti-hTfR antibody, pabinafusp alfa, for MPS-II: a phase 2 trial in Brazil, Mol. Ther. 29 (2021) 2378–2386, https://doi.org/10.1016/j.ymthe.2021.03.019.

[20] G.C. Terstappen, A.H. Meyer, R.D. Bell, W. Zhang, Strategies for delivering therapeutics across the blood–brain barrier, Nat. Rev. Drug Discov. 20 (2021) 362–383, https://doi.org/10.1038/s41573-021-00139-y.

[21] A. Mullard, Blood–brain barrier-traversing biologic secures regulatory approval, in Japan, Nat. Rev. Drug Discov. 20 (2021) 332, https://doi.org/10.1038/d41573-021-00066-y.

[22] X.T. Fang, G. Hultqvist, S.R. Meier, G. Antoni, D. Sehlin, S. Syvänen, High detection sensitivity with antibody-based PET radioligand for amyloid beta in brain, Neuroimage 184 (2019) 881–888, https://doi.org/10.1016/j.neuroimage.2018.10.011.

[23] S. Syvänen, X.T. Fang, R. Faresjö, J. Rokka, L. Lannfelt, D.E. Olberg, J. Eriksson, D. Sehlin, Fluorine-18-Labeled antibody ligands for PET imaging of amyloid-β in brain, ACS Chem. Neurosci. 11 (2020) 4460–4468, https://doi.org/10.1021/acschemneuro.0c00652.

[24] G. Bonvicini, S. Syvänen, K.G. Andersson, M. Haaparanta-Solin, F. López-Picón, D. Sehlin, ImmunoPET imaging of amyloid-beta in a rat model of Alzheimer's disease with a bispecific, brain-penetrating fusion protein, Transl. Neurodegener. 11 (2022) 1–14, https://doi.org/10.1186/s40035-022-00324-y.

[25] T.E. Wuensche, N. Stergiou, I. Mes, M. Verlaan, M. Schreurs, E.J.M. Kooijman, B. Janssen, A.D. Windhorst, A. Jensen, A.A. Asuni, B. Bang-Andersen, W. Beaino, G. A.M.S. Dongen, D.J. Vugts, Advancing 89Zr-immuno-PET in neuroscience with a bispecific anti-amyloid-beta monoclonal antibody – the choice of chelator is essential, Theranostics 12 (2022) 7067–7079, https://doi.org/10.7150/thno.73509.

[26] N. Stergiou, T.E. Wuensche, M. Schreurs, I. Mes, M. Verlaan, E.J.M. Kooijman, A. D. Windhorst, L. Helboe, S. Vergo, S. Christensen, A.A. Asuni, A. Jensen, G.A.M. S. Van Dongen, B. Bang-Andersen, D.J. Vugts, W. Beaino, Application of 89Zr-DFO*-immuno-PET to assess improved target engagement of a bispecific anti-amyloid-ß monoclonal antibody, Eur. J. Nucl. Med. Mol. Imag. 50 (2023) 1306–1317, https://doi.org/10.1007/s00259-023-06109-3.

[27] R. Faresjö, G. Bonvicini, X.T. Fang, X. Aguilar, D. Sehlin, S. Syvänen, Brain pharmacokinetics of two BBB penetrating bispecific antibodies of different size, Fluids Barriers CNS 18 (2021) 1–15, https://doi.org/10.1186/s12987-021-00257-0.

[28] R.J. Boado, Q.H. Zhou, J.Z. Lu, E.K.W. Hui, W.M. Pardridge, Pharmacokinetics and brain uptake of a genetically engineered bifunctional fusion antibody targeting the mouse transferrin receptor, Mol. Pharm. 7 (2010) 237–244, https://doi.org/10.1021/mp900235k.

[29] C.I. Webster, J. Hatcher, M. Burrell, G. Thom, P. Thornton, I. Gurrell, I. Chessell, Enhanced delivery of IL-1 receptor antagonist to the central nervous system as a novel anti-Transferrin receptor-IL-1RA fusion reverses neuropathic mechanical hypersensitivity, Pain 158 (2017) 660–668, https://doi.org/10.1097/j.pain.0000000000000810.

[30] P. Stocki, J. Szary, C.L.M. Rasmussen, M. Demydchuk, L. Northall, D.B. Logan, A. Gauhar, L. Thei, T. Moos, F.S. Walsh, J.L. Rutkowski, Blood-brain barrier transport using a high affinity, brain-selective VNAR antibody targeting transferrin receptor 1, FASEB (Fed. Am. Soc. Exp. Biol.) J. 35 (2021) 1–19, https://doi.org/10.1096/fj.202001787R.

[31] Y. Zhang, J. Yu Zuchero, J. Atwal, J. Couch, M.S. Dennis, J.A. Ernst, R.J. Watts, G. A. Lazar, Anti-transferrin Receptor Antibodies and Methods of Use, US 9,708.406 B2, 2017.

[32] Q.H. Zhou, J.Z. Lu, E.K.W. Hui, R.J. Boado, W.M. Pardridge, Delivery of a peptide radiopharmaceutical to brain with an IgG-avidin fusion protein, Bioconjugate Chem. 22 (2011) 1611–1618, https://doi.org/10.1021/bc200174x.

[33] B. van Lengerich, L. Zhan, D. Xia, D. Chan, D. Joy, J.I. Park, D. Tatarakis, M. Calvert, S. Hummel, S. Lianoglou, M.E. Pizzo, R. Prorok, E. Thomsen, L. M. Bartos, P. Beumers, A. Capell, S.S. Davis, L. de Weerd, J.C. Dugas, J. Duque, T. Earr, K. Gadkar, T. Giese, A. Gill, J. Gnörich, C. Ha, M. Kannuswamy, D.J. Kim, S.T. Kunte, L.H. Kunze, D. Lac, K. Lechtenberg, A.W.S. Leung, C.C. Liang, I. Lopez, P. McQuade, A. Modi, V.O. Torres, H.N. Nguyen, I. Pesämaa, N. Propson, M. Reich, Y. Robles-Colmenares, K. Schlepckow, L. Slemann, H. Solanoy, J.H. Suh, R. G. Thorne, C. Vieira, K. Wind-Mark, K. Xiong, Y.J.Y. Zuchero, D. Diaz, M.S. Dennis, F. Huang, K. Scearce-Levie, R.J. Watts, C. Haass, J.W. Lewcock, G. Di Paolo, M. Brendel, P.E. Sanchez, K.M. Monroe, A TREM2-activating antibody with a blood–brain barrier transport vehicle enhances microglial metabolism in Alzheimer's disease models, Nat. Neurosci. 26 (2023) 416–429, https://doi.org/10.1038/s41593-022-01240-0.

[34] M.S. Thomsen, K.B. Johnsen, K. Kucharz, M. Lauritzen, T. Moos, Blood–brain barrier transport of transferrin receptor-targeted nanoparticles, Pharmaceutics 14 (2022) 1–17, https://doi.org/10.3390/pharmaceutics14102237.

[35] D. Wu, W.M. Pardridge, Neuroprotection with noninvasive neurotrophin delivery to the brain, Proc. Natl. Acad. Sci. U.S.A. 96 (1999) 254–259, https://doi.org/10.1073/pnas.96.1.254.

[36] M.S. Kariolis, R.C. Wells, J.A. Getz, W. Kwan, C.S. Mahon, R. Tong, D.J. Kim, A. Srivastava, C. Bedard, K.R. Henne, T. Giese, V.A. Assimon, X. Chen, Y. Zhang, H. Solanoy, K. Jenkins, P.E. Sanchez, L. Kane, T. Miyamoto, K.S. Chew, M.E. Pizzo, N. Liang, M.E.K. Calvert, S.L. DeVos, S. Baskaran, S. Hall, Z.K. Sweeney, R. G. Thorne, R.J. Watts, M.S. Dennis, A.P. Silverman, Y.J.Y. Zuchero, Brain delivery

of therapeutic proteins using an Fc fragment blood-brain barrier transport vehicle in mice and monkeys, Sci. Transl. Med. 12 (2020) 1–13, https://doi.org/10.1126/scitranslmed.aay1359.

[37] E. Wijaya, C. Lenaerts, S. Maricot, J. Hastanin, S. Habraken, J.P. Vilcot, R. Boukherroub, S. Szunerits, Surface plasmon resonance-based biosensors: from the development of different SPR structures to novel surface functionalization strategies, Curr. Opin. Solid State Mater. Sci. 15 (2011) 208–224, https://doi.org/10.1016/j.cossms.2011.05.001.

[38] S.A. Hunter, J.R. Cochran, Cell-binding assays for determining the affinity of protein–protein interactions: Technologies and considerations, in: Methods Enzymol, Academic Press Inc., 2016, pp. 21–44, https://doi.org/10.1016/bs.mie.2016.05.002.

[39] S.W. Meister, L.C. Hjelm, M. Dannemeyer, H. Tegel, H. Lindberg, S. Ståhl, J. Löfblom, An affibody molecule is actively transported into the cerebrospinal fluid via binding to the transferrin receptor, Int. J. Mol. Sci. 21 (2020) 1–14, https://doi.org/10.3390/ijms21082999.

[40] H. Cohen-Dvashi, R. Amon, K.N. Agans, R.W. Cross, A. Borenstein-Katz, M. Mateo, S. Baize, V. Padler-Karavani, T.W. Geisbert, R. Diskin, Rational design of universal immunotherapy for TfR1-tropic arenaviruses, Nat. Commun. 11 (2020) 1–11, https://doi.org/10.1038/s41467-019-13924-6.

[41] D.J. Sjöström, S.A. Berger, G. Oberdorfer, S. Bjelic, Computational backbone design enables soluble engineering of transferrin receptor apical domain, Proteins: Struct., Funct., Bioinf. 88 (2020) 1569–1577, https://doi.org/10.1002/prot.25974.

[42] K. Kissel, S. Hamm, M. Schulz, A. Vecchi, C. Garlanda, B. Engelhardt, Immunohistochemical localization of the murine transferrin receptor (TfR) on blood-tissue barriers using a novel anti-TfR monoclonal antibody, Histochem. Cell Biol. 110 (1998) 63–72, https://doi.org/10.1007/s004180050266.

[43] J.A. Couch, Y.J. Yu, Y. Zhang, J.M. Tarrant, R.N. Fuji, W.J. Meilandt, H. Solanoy, R.K. Tong, K. Hoyte, W. Luk, Y. Lu, K. Gadkar, S. Prabhu, B.A. Ordonia, Q. Nguyen, Y. Lin, Z. Lin, M. Balazs, K. Scearce-Levie, J.A. Ernst, M.S. Dennis, R.J. Watts, Addressing safety liabilities of TfR bispecific antibodies that cross the blood-brain barrier, Sci. Transl. Med. 5 (2013) 1–12, https://doi.org/10.1126/scitranslmed.3005338.

[44] C.M. Lawrence, S. Ray, M. Babyonyshev, R. Galluser, D.W. Borhani, S.C. Harrison, Crystal structure of the ectodomain of human transferrin receptor, Science 286 (1999) 779–782, https://doi.org/10.1126/science.286.5440.779.